Journal of Visualization manuscript No.
(will be inserted by the editor)

Mixing of a Two-Layer Density-Stratified Fluid by Two Vortex Rings Successively Launched towards the Density Interface

Lile Cao · Kotaro Takamure · Tomohiro Degawa · Tomomi Uchiyama

Received: date / Accepted: date

Abstract In this study, two vortex rings composed of upper fluid were continuously ejected vertically downward toward the interface of the two-layer density stratified fluid. The motion of the vortex rings and behavior of the lower layer fluid were investigated via visualization experiment, and the effect of time interval between the injections of the two vortex rings on the mixing of the density stratified fluid was investigated. The first emitted vortex ring (VR_A) advected vertically downward in the upper layer, passed through the density interface, and then advected in the lower layer. After VR_A reached the maximum depth in the lower layer, the upper part of the fluid mass ejected into the upper layer due to buoyancy. The lower fluid was entrained in the upper layer. Subsequently, a new vortex ring (VR_C) was generated by the fluid mass ejected in the upper layer and advected vertically upward in the upper layer. The second vortex ring emitted (VR_B) collided with the tip of the fluid mass of the VR_A ejected from the lower layer. Subsequently, it slightly penetrated the lower layer, rolled up the lower layer fluid into the upper layer, and coalesced with VR_C to collapse. In the process of vortex merging, the mixing of the upper and lower layers reached a maximum when the VR_A reached the maximum depth. Furthermore, it was clarified that the mixing ability of the upper and lower layers depends on the ejection time interval of the two vortex rings.

Keywords Density-stratified fluid · Mixing · Vortex ring · Density interface · PLIF

Lile Cao

Graduate School of Informatics, Nagoya University, Furo-cho, Chikusa-ku, Nagoya 464-8601, Japan

Tel.: +81-52-789-4219

Fax: +81-52-789-4219

E-mail: cao.lile@k.mbox.nagoya-u.ac.jp

Tomomi Uchiyama

uchiyama@is.nagoya-u.ac.jp

Declarations

Funding

Not applicable

Conflicts of interest/Competing interests

The author declares that there are no conflicts of interest.

Availability of data and material

The data that support the findings of this study are available from the corresponding author, Lile Cao, upon reasonable request.

Code availability

Not applicable

Authors' contributions

Investigation: Lile Cao; Writing - original draft: Lile Cao; Formal analysis: Lile Cao, Kotaro Takamure; Methodology: Tomohiro Degawa; Writing - review & editing: Kotaro Takamure, Tomomi Uchiyama; Supervision: Tomomi Uchiyama.

1 Introduction

Liquefied natural gas (LNG) is considered a clean energy source because it emits less greenhouse gases, such as CO_2, and atmospheric pollutants, such as NO_X, than coal and petroleum when it is burned. In addition, natural gas is widely distributed around the world and has a longer useful life than petroleum. Hence, it is expected to be an energy source that can be stably supplied in the future. LNG exports are expected to continue to increase in Australia and the US, and LNG imports are expected to increase in China, India, and Europe (IEA 2019). Given the characteristics of LNG described above, it is assumed that the demand for LNG will continue to increase worldwide in the future.

Furthermore, LNG imported by tankers is stored in tanks at the receiving terminal, regasified, and then shipped as fuel for power generation and raw material for city gas. To efficiently use storage tanks, LNG from different production areas is mixed and stored in one tank and is widely used. The density and composition of LNG depends on the production area. Thus, LNG is stratified, which in turn forms a density stratification in an LNG storage tank. The density of stratified LNG changes when heat is input from the outside of the tank and when the components of LNG change over time. When the densities of the upper and lower layers become equal, a rapid mixing phenomenon called rollover occurs. During this process, a large amount of LNG vaporizes, which can cause deformation, damage, or destruction of the LNG tank (Bates and Morrison 1997). The rollover that occurred at the LNG terminal in Italy in 1971 was serious; thus, rollover has become the focus of many studies. Currently, prevention and elimination of stratification is an important technology for the operation of LNG storage tanks.

To prevent and eliminate stratification in LNG tanks, a promising method involves using a nozzle installed at the bottom or top of the tank to inject LNG into the tank via a pump, and this promotes stirring and mixing. To date, various laboratory experiments (Baines et al. 1990; Bloomeld and Kerr 1998; Lin and Linden 2005; Ansong et al. 2008) have been conducted to investigate the interaction between the interface of the dense stratified fluid and the jet. In a previous study (Degawa et al. 2017, 2018a, b), the authors stored a two-layer stratified fluid consisting of water in the upper layer and an aqueous solution of sodium chloride in the lower layer in a cylindrical tank. They jetted the lower layer fluid 60° upward from the nozzle at the bottom. The mixing phenomenon of the flow and upper and lower layers were investigated via experiments and simulations. The mixing process due to the jet was visualized in vertical and horizontal sections, and the effect of Reynolds number Re of the jet on the mixing was clarified (Degawa et al. 2017). The flow field and concentration field in the tank investigated in the experiment (Degawa et al. 2017) were analyzed via simulations. The findings supplemented the experimental results and aided in understanding the secondary flow generated in the horizontal section (Degawa et al. 2018a). The concentration distribution in the vertical section of the tank was measured by the PLIF method, and the effect of Re on the behavior of the jet and mixing process was also clarified (Degawa et al. 2018b).

Conversely, a fluid mass in which the vorticity is concentrated in a torus shape is termed as a vortex ring. The vortex ring has the characteristics of vortical motion that entrains matter inside and exhibits convective motion, which transports the matter. The authors (Uchiyama et al., 2017a, b) experimentally investigated the possibility of controlling the motion of bubbles and solid particles via vortex rings in water. Uchiyama and Kusamichi (2017a) injected bubbles (mean diameter: 3.44 mm) into the vortex core during ejection of the vortex ring in still water. If the strength of the vortex ring is large enough, then the vortex ring can capture the bubbles to form a cluster of bubbles and transport them over a certain distance. Based on these findings, it can be expected that the vortex ring ejected toward the density interface of the density stratified fluid can lead to the mixing of the upper and lower layers and eliminate the stratification. Previously, the interaction between the vortex ring and density interface was experimentally investigated, and it was reported that it can be arranged in dimensionless quantities such as the Reynolds number, Froude number, Atwood number, and Richardson number (Linden, 1973; Dahm et al., 1989; Camassa et al., 2013; Advaith et al., 2017).

Visualization experiments on the interaction between the vortex ring and density interface were conducted (Tsunoda et al., 2011), and the effect of the density ratio on the deformation of the vortex ring due to the interaction was clarified.

The velocity distribution of the vortex ring was also measured, and the instability of the vortex ring due to collision was shown (Olsthoorn and Dalziel, 2017). Additionally, simulations of the interaction between the vortex ring and density interface were performed to complement experimental research (Camassa et al., 2013; Stock et al., 2008; Marcus and Bell, 1994; Robins and Delisi, 1998). However, there is a paucity of studies focusing on the mixing of the upper and lower layers via the vortex ring. Therefore, in a previous study (Cao et al., 2019), the authors stored a two-layer density stratified fluid with water in the upper layer and aqueous sodium chloride solution in the lower layer in a rectangular tank. The vortex ring, which was composed of water, was launched from the circular orifice vertically downward toward the density interface. The relative motion of the vortex ring with respect to the interface and the behavior of the lower fluid were visualized. The mixing phenomenon of the upper and lower layers due to the vortex ring was investigated. The Atwood number, which denotes the amount of density jump at the interface, was 0.0055, and the Reynolds number Re based on the circulation of the vortex ring and kinematic viscosity of water was 1073, 1342, and 1610. Thus, it was visualized that the vortex ring advances vertically downward in the upper layer fluid and penetrates the density interface. Furthermore, it bounces toward the interface and collapses when it reaches a certain depth in the lower layer fluid. It was shown that the depth increases with Re. Additionally, the mixing index was defined based on the concentration distribution in the tank, and it attains a maximum value when the vortex ring reaches the maximum depth in the lower fluid. Subsequently, the vortex ring rebounded and entrained the lower layer fluid into the upper layer fluid and then gradually decreased. The details of the relationship between vortex ring motion and mixing around the density interface were clarified. This study demonstrates the utility of vortex rings for mixing density stratified fluids. It is expected that a higher mixing effect will be realized when vortex rings are continuously launched from the same orifice at regular time intervals. However, there is a paucity of studies that focus on the mixing process via vortex rings that are continuously injected at the density interface and the interaction between the vortex rings and density interface. In this study, by using the same experimental device as that in study (Cao et al., 2019), two vortex rings composed of the upper fluid were continuously ejected vertically downward toward the interface of the two-layer density stratified fluid. The motion of the vortex rings and behavior of the lower layer fluid were investigated via a visualization experiment, and the effect of the time interval between the injections of the two vortex rings on the mixing of the density stratified fluid was clarified.

2. Experimental setup, method, and conditions

2.1 Experimental setup

Figure 1 shows a schematic of the experimental setup. At the initial time ($t = 0$), a two-layer density stratified fluid with water in the upper layer and aqueous sodium chloride solution (NaCl) in the lower layer was stationary inside the rectangular tank. This stratified fluid was formed using the method described below. First, an aqueous solution of sodium chloride was filled to a predetermined height in the tank. After the sodium chloride aqueous solution became stationary, a sponge was placed on the liquid surface and water was poured from the top of the sponge. By using this method, it was possible to form a density stratified fluid with a horizontal interface whose density changes sharply in the vertical direction. The tank was fabricated from transparent acrylic resin to visualize the fluid. A device consisting of a cylinder and piston was installed on the center of the top surface of the tank to launch the vortex ring. The center axis of the cylinder was parallel to the vertical axis. A circular orifice was attached to the cylinder outlet. The orifice was located inside the upper fluid. The center of the orifice outlet corresponded to the origin of the coordinates, the x-axis was in the horizontal plane, and the y-axis was vertically downward. Multiple vortex rings were ejected vertically downward toward the density interface by driving the piston with an actuator incorporating a brushless DC motor into the upper layer fluid (water).

Figure 2 shows the dimensions of each part of the experimental setup. The width and depth of the rectangular tank were 280 mm, and the height was 340 mm. The thicknesses of the upper layer (water) and lower layer (NaCl) were 60 mm and 230 mm, respectively. The diameter of the piston was 42.7 mm and the stroke length was 1.73 mm. The piston was stationary at time t = 0, and the z coordinate of its tip corresponded to 30 mm. The diameter d of the orifice was 10 mm and the thickness was 5 mm. The orifice outlet was located 10 mm below the upper fluid surface.

2.2 Experimental method

Two vortex rings were launched with a time interval Δt. First, at t = 0, the interior of the cylinder was filled with water containing the fluorescent dye Rhodamine B, and the piston was pushed down to eject the first vortex ring from the orifice into the upper layer (water). Next, at $t = \Delta t$, the piston was pushed down again, and the second vortex ring was injected. Given that the pushing speed and stroke of the piston for the leading and trailing vortex rings were the same, the strengths of the two vortex rings were equal. Hereafter, the leading and trailing vortex rings are denoted as VR_A and VR_B, respectively.

A fluorescent dye eosin was added to the lower layer fluid. The amount of fluorescent dye that was added corresponded to 0.85 g/m^3, and the temperature of the stratified fluid was 298 K. Fig. 1 shows that a laser sheet (power 100 mW, wavelength 532 nm, thickness 1 mm) is irradiated from the bottom of the tank. Subsequently, the vortex ring and lower layer fluid in the x – z plane were visualized via the PLIF method. Two digital cameras, A and B, were installed at the height (z/d = 5) of the density interface across the x- z plane, and the x-z plane inside the tank was photographed simultaneously. Images of the vortex ring visualized via Rhodamine B and the lower layer fluid visualized via Eosin were acquired using camera A. Furthermore, camera B was equipped with a bandpass filter, and only the visualized image of the lower layer fluid was acquired. The image resolution was 1920 × 1080 pixels, frame rate was 30 fps, and shutter speed was 1/60 s.

The concentration of the lower layer fluid was estimated from the fluorescence intensity of eosin, which was measured using camera B (Degawa et al., 2018b; Cao et al., 2019). The maximum and minimum values of fluorescence intensity in the image were regarded as the maximum and minimum densities, respectively. Concentration C was calculated by assuming that there is a linear relationship between fluorescence intensity and concentration.

In this study, we adopted the mixing index θ, which was used in a previous study (Cao et al., 2019), to evaluate the mixing of the upper and lower layers via a single vortex ring. The mixing index θ was defined as

$$\theta(t) = \frac{1}{2\alpha\beta(1-\alpha)L_Z}\int_0^{L_z}\left|\overline{C}(z) - \overline{C}_0(z)\right|dz \tag{1}$$

where $\overline{C}$ denotes the average value of C in the horizontal plane at height z and time t, $\overline{C}_0$ denotes the value of $\overline{C}$ when t = 0, L_z denotes the thickness (290 mm) of the density-stratified fluid. Furthermore, α denotes the ratio of the initial thickness of the lower layer fluid to L_z (230/290), and β denotes the initial concentration of the lower fluid (β = 0.02).

The mixing ability $\hat{\theta}$ of the vortex ring is defined by the following equation:

$$\hat{\theta} = \int_0^{t_s}\theta(t)dt \tag{2}$$

where, t_s denotes the time when θ reaches a steady state.

2.3 Experimental conditions

The strength of the vortex ring (circulation Γ) is defined by the following equation, which is similar to that in the vortex ring experiments conducted by Glezer (1988) and other previous studies (Uchiyama et al., 2017a,b; Cao et al., 2019).

$$\Gamma = \int_0^T \frac{{u_0}^2}{2} dt \quad (3)$$

where, T denotes the time for the piston to press down, and u_0 denotes the fluid velocity at the outlet of the orifice. In this experiment, $u_0 = 0.076$ m/s.

The Reynolds number Re of the vortex ring is defined by Γ/ν, where ν denotes the kinematic viscosity of the upper fluid (water). The relationship between u_0 and Γ is given by Eq. (3). Thus, in this study, Re = Γ/ν, was determined by reducing the piston variable speed.

Dahm et al. (1989) and Tsunoda et al. (2011) expressed experimental conditions via density changes at the interface and Froude numbers when investigating the interaction between vortex rings and density interfaces. Atwood number A (representing the difference between the densities) and the Froude number Fr (representing the ratio of the inertial force to the gravity of the vortex ring) are expressed as follows:

$$\mathrm{A} = \frac{\rho_2 - \rho_1}{\rho_1 + \rho_2} \quad (4)$$

$$\mathrm{Fr} = \frac{\Gamma^2}{gD^3} \quad (5)$$

where g denotes the gravitational acceleration. Furthermore, ρ_1 and ρ_2 denote the densities of the upper and lower layers, respectively. Specifically, D denotes the distance between two vortex core centers (the vortex ring diameter) in the x–z plane.

In this study, the concentration of the lower fluid (NaCl) was 0.02. Therefore, A = 0.0055 and Re (= Γ/ν) = 1342. As discussed later, given that D near the orifice outlet was 1.25 d, Fr = 0.11. The Richardson number Ri (=A/Fr), which is the ratio of the buoyancy force to the inertial force of the vortex ring, was 0.049.

Time t is a dimensionless value t^* (= u_0t/d), which is based on the velocity u_0 of the fluid at the orifice outlet and orifice diameter d. The dimensionless values of Δt^* (= $u_0\Delta t/d$)) over the time interval Δt of the two vortex rings were 9.6, 16.5, and 22. In this experiment, the shortest time for the second vortex ring to be launched is 9.6 because the linear actuator should move back to generate the 2nd vortex ring. In past experiments performed by Cao et al. (2019) for a single vortex ring in the case of Re = 1342, at t^* = 22, the 1st vortex ring bounced back to the upper fluid and after that crashed. So, if time is longer than 22, the effect of 1st vortex ring can be ignored. 16.5 was choose as a time between 9.6 and 22, which is also a selectable time for linear actuator. The experimental conditions are summarized in Table 1. For each experimental case, more than 5 times were performed and similar phenomena were observed. Typical results of each case are shown in this paper.

2.4 Vortex ring displacement and diameter

The displacements of the 1st vortex ring VR_A and 2nd vortex ring VR_B are shown in Fig. 3, which is an example of a visualized image. The distance from the orifice outlet to the plane of vortex core of VR_A and VR_B is denoted by z_A and z_B, respectively. The diameters VR_A and VR_B are regarded as the distance between two vortex cores in the visualized image and are denoted as D_A and D_B, respectively.

3. Results and discussion

3.1 Behavior of the 1st vortex ring VR_A

Figure 4 shows the images visualized by camera A when the vortex ring ejection time interval Δt^* = 9.6. The water ejected from the orifice and lower fluid were visualized with rhodamine B and eosin, respectively. At time t^* = 3.8, a shear layer appeared at the boundary between the water sprayed from the orifice and stationary water in the tank, and the vortex ring VR_A was generated due to the rolling up. At t^* = 7.6, the VR_A was advected vertically downward toward the density interface. At t^* = 11.4, the entire VR_A invaded the lower layer. Subsequently, the vortex ring VR_B was formed at the exit of the orifice. At $t^* = 15.2$, the VR_A deeply penetrated vertically in the lower layer. Given the buoyancy in the lower layer, the VR_A composed of the upper fluid layer (water) was stretched vertically, and the upper end of the VR_A was blown up from the density interface into the upper layer. During this process, a small amount of lower layer fluid was entrained in the upper layer. Additionally, VR_B was advected vertically downward toward the density interface. At these four times, the vortex cores of the VR_A and VR_B were clearly visualized. However, at $t^* > 15.2$, the VR_A was significantly deformed and the vortex cores became unclear.

Figure 5 shows the visualized images when $\Delta t^* = 16.5$. The results are shown at the same dimensionless time as that in Fig. 4. At $t^* = 3.8$, 7.6, and 11.4, the same VR_A as that when $\Delta t^* = 9.6$ was visualized. At $t^* = 15.2$, the VR_A was stretched and its upper end was blowing up into the upper layer. When $t^* > 15.2$, the VR_A was significantly deformed and the vortex core became unclear. In the case when $\Delta t^* = 22$, VR_A behaves similarly to the case when $\Delta t^* = 16.5$ and $t^* \leq 15.2$ because VR_B is not ejected yet. When $\Delta t^* = 9.6$, VR_B approaches VR_A, as shown in Fig. 4 (d). However, the state of the VR_A stretched in the vertical direction is almost the same as that in the case when $\Delta t^* = 16.5$ and 22. Therefore, under the conditions of this experiment, when $t^* \leq 15.2$, it was observed that the effect of VR_B on VR_A is extremely small.

The displacement z_A of the 1st vortex ring VR_A is obtained from the visualized image, and the time variation of the displacement z_A/d is shown in Fig. 6. The figure shows the result at time $t^* \leq 15.2$ when the vortex core is clearly observed. Furthermore, VR_A advects at an almost constant velocity in the upper layer ($0 \leq z_A/d \leq 5$) irrespective of the value of the vortex ring injection time interval Δt^*. The effect of Δt^* on the advection velocity is almost zero. In the case of $\Delta t^*= 9.6$, the trailing vortex ring VR_B approaches VR_A at $11.4 \leq t^* \leq 15.2$, as shown in Fig. 4. The distance between the vortex rings was large. Hence, the effect of VR_B did not appear on the movement of the VR_A. In the lower layer ($z_A/d > 5$), the advection velocity decreased slightly due to the effect of buoyancy. At $t^* = 15.2$, the VR_A reached the maximum depth in the lower layer.

The diameter of the vortex ring D_A, which is the distance between VR_A vortex cores, is shown as a dimensionless value D_A/d in Fig. 7 with a displacement of z_A/d. Specifically, D_A/d was almost constant in the upper layer ($0 \leq z_A/d \leq 5$) and does not depend on the time interval Δt^*. The average value of D_A in the upper layer was 1.25 d. However, at $z_A/d \geq 5.4$ in the lower layer, D_A/d decreased significantly with an increase in penetration depth (z_A). A similar tendency was observed in the experiment by Advaith et al. [16]. In the lower layer (NaCl), owing to the buoyancy acting on the VR_A, the vertical movement of the VR_A was resisted. Therefore, as shown in Fig. 4 and Fig. 5, the vortex rings were stretched in the vertical direction. Immediately after the rapid decrease of D_A, the vortex ring was deformed and the vortex core became unclear, and thus it was difficult to measure D_A.

3.2 interaction between 1st vortex ring (VR_A) and 2nd vortex ring (VR_B)

Figure 8 shows the visualized images of the lower layer fluid and two vortex rings that are continuously ejected in the case $\Delta t^* = 9.6$. At time $t^* = 12.9$, the VR_B advanced vertically downward in the lower layer and maintained an axisymmetric shape. At this time, the VR_B advanced downward in the upper layer toward the density interface. At $t^* = 15.2$, the VR_A reached the maximum depth. However, it was stretched vertically due to buoyancy during advection. Owing to this buoyancy, the upper edge of the fluid mass (water mass) of the VR_A blew up into the upper layer, and the surrounding lower fluid was entrained in the upper layer. Given that the surface of the fluid mass rising in the upper layer corresponds to the shear layer, the tip of the fluid mass rolled up. At $t^* = 16.7$, the VR_A and fluid mass at the upper edge floated, and the entrainment of the lower layer fluid into the upper layer became significant. The tip of this fluid mass and VR_B collided slightly above the density interface. At $t^* = 18.2$. owing to the collision of the vortex rings, the VR_B moved in the horizontal (x) direction while entraining the fluid mass of the VR_A . Hence, the diameter of the VR_B increased. At the same time, the rolling up of the fluid mass of VR_A formed another vortex ring, which was in contact with the outside of the VR_B.

Hereinafter, the newly formed vortex ring is termed as VR_C. The rotation direction of the VR_C is opposite to that of the VR_B. The VR_A in the lower layer continued to float. At t^* = 19.8, the VR_C separated from the VR_B. At this time, the VR_A existed in the lower layer and the VR_B and VR_C existed in the upper layer. For t^* = 21.3 to 22.8, VR_A reached the density interface and disappeared. The VR_C moved in the direction of the central axis (x = 0). At t^* = 26.6, the VR_B penetrated slightly into the lower layer, merged with the VR_C, and then the large-scale vortex structure collapsed. Therefore, the lower layer fluid was rolled up in the upper layer. At $t^* \geq 40.3$, the vortex structure became finer and the density interface became horizontal.

Figure 9 shows the visualized images of the vortex rings when Δt^* = 16.5. At time t^* = 12.9, the VR_A was advancing vertically downward in the lower layer while maintaining its axisymmetric shape. At t^* = 19, after the VR_A reached the maximum depth, the fluid mass above the VR_A was blowing up into the upper layer. Furthermore, the VR_C was generated at the tip of the fluid mass owing to the rolling up of the shear layer. The shape of the VR_A was non-axisymmetric, and the vortex cores could not be identified. The VR_B was advancing vertically downward toward the VR_C. At t^* = 21.3, the developed VR_C interacted with the VR_B. The VR_C entrained the lower layer fluid around the vortex core and the VR_A disappeared in the lower layer. From t^* = 22 to 25.1, the VR_B moved towards the density interface while excluding the VR_C to the outside and reached the interface at t^* = 27.4. Furthermore, the VR_B advected downward in the lower layer at t^* = 32.7. Subsequently, it deformed and collapsed, when it was rising due to buoyancy, and became a minute vortex.

Figure 10 shows the visualized images when Δt^* = 22. At t^* = 12.9, the VR_A maintained axial symmetry in the lower layer. At t^* = 21.3, the fluid mass of the VR_A increased owing to buoyancy and generated VR_C in the upper layer. The lower fluid was entrained around the vortex core of the VR_C. At t^* = 24.3, the VR_C moved up and the VR_B decreased. At t^* = 25.8, VR_B interacted with VR_C. From t^* = 26.6 to 29.6, the VR_B descended toward the density interface as VR_C attenuated behind it. At t^* = 36.5, it penetrated into the lower layer. After that, the VR_B was moving up due to buoyancy and collapsed in the upper layer from t^* = 43.3 to 63.1

Figure 11 shows the time variation of displacement z_B of the 2nd VR_B. However, the displacement was measured at the time when the vortex core was clearly visualized. Hence, it was limited to the result in the upper layer ($0 \leq z_B/d \leq 5$). For reference, the displacement of the 1st vortex ring VR_A is also shown in the plot in Fig. 11. The result corresponded to the time until t^* = 17.1, which was immediately before the collision of the fluid mass that formed the VR_A and VR_B at Δt^* = 9.6. The VR_B advected in the upper layer at a nearly constant velocity, and the speed was almost the same as that of the VR_A. Therefore, it was not affected by the VR_A. In the case of Δt^* = 16.5, the speed decreased at t^* = 21.5. This is because the VR_B collided head-on with VR_C based on the image visualized at approximately the same time (Fig. 9 (c)). The speed decreased sharply at t^* = 23.8. This because the VR_B advanced towards the density interface while excluding the VR_C to the outside (see Fig. 9 (e)). The speed also decreased at $t^* \geq 23.8$, and the maximal depth of the VR_B became lower that that at Δt^* = 9.6. This is because it interacted with the VR_C, as shown in Figs. 9 (f) and (g). In the case of Δt^* = 22, the velocity decreased at t^* = 25. The reason is evident in Fig. 10 (d), where the VR_B collided with the VR_C. At $t^* \geq 25$, the velocity was almost constant. In Figs. 10 (e), (f), and (g), the VR_B interacts with the VR_C after they collide with each other. As time passed after the VR_C was generated, the strength of the VR_C was not sufficient to decelerate the VR_B.

Figure 12 shows the variation in the diameter D_B with respect to the displacement z_B of the VR_B. In the case of Δt^* = 9.6, D_B rapidly increased at $z_B/d \simeq 4$. As shown in Fig. 8 (c), VR_B collides with the upper end of the fluid mass of the VR_A at z_B/d = 4, and the vortex cores move outward. The increase in the vortex ring diameter due to such collisions was also reported in the simulation by Meinke et al. [24]. When Δt^* = 16.5 and 22, D_B rapidly increased and then decreased at approximately $z_B/d \simeq 3.3$. At $z_B/d \simeq 3.3$, the VR_B collides with the VR_C, as shown in Fig. 9 (c) and Fig. 10 (e). Furthermore, it was evident that the diameter of the VR_B increased after the collision with the VR_C and decreased with the elimination of the VR_C to the outside.

3.3 Behavior of lower fluid and mixing index

The images of the lower layer fluid visualized with eosin were acquired using camera B. Fig. 13 shows the images when Δt^* = 9.6. At t^* = 12.9, the 1st vortex ring VR_A penetrated deeply into the lower layer (see Fig. 8 (a)). Furthermore, t^* = 22.8 is the time when VR_B approaches the density interface (see Fig. 8 (g)), and the mixing of the upper and lower fluids near the interface is low. At t^* = 26.6, the VR_B slightly penetrates into the lower layer and collapses above the interface (see Fig. 8 (h)), and the lower layer fluid is rolled up in the upper layer. At t^* = 40.3, the large-scale vortex structure disappears (see Fig. 8 (i)), and the mixing near the interface almost stops.

Figure 14 shows the behavior of the lower fluid when Δt^* = 16.5. At t^* = 12.9, the VR_A penetrates deeply into the lower layer (see Fig. 9 (a)). At t^* = 27.4, the VR_B approaches the density interface (see Fig. 9 (g)), and the mixing of the upper and lower fluids near the interface is low. At t^* = 32.7, VR_B penetrates into the lower layer (see Fig. 9 (h)). At t^* = 38.8, the VR_B floating from the lower layer to the upper layer collapses (see Fig. 9 (i)), and the mixing near the density interface almost stops.

Figure 15 shows the behavior of the lower fluid when Δt^* = 22. At t^* = 12.9, VR_A penetrates deeply into the lower layer (see Fig. 10 (a)). At t^* = 29.6, the VR_B approaches the density interface (see Fig. 10 (g)), and the lower fluid entrained by the VR_C exists slightly above the density interface. At t^* = 36.5, VR_B enters the lower layer (see Fig. 10 (h)), and the lower layer fluid remains in the upper layer. At t^* = 43.3, the VR_B levitates in the upper layer and collapses (see Fig. 10 (i)), and the upper layer fluid does not enter the lower layer.

The mixing index, θ, is calculated from Eq. (1). Furthermore, θ with respect to the dimensionless time t^* is shown in Fig. 16. The times of the visualized images in Figs. 13 to 15 are shown by symbols (a) to (d). In the case of Δt^* = 9.6, θ increases and decreases. The maximum value is obtained at t^* = 12.9 because the VR_A that consists of the upper fluid penetrates deeply into the lower fluid (see Fig. 13 (a)). It becomes a minimum at t^* = 22.8 because the mixing of the upper and lower fluids near the interface is low (see Fig. 13 (b)). At t^* = 26.6, the maximum value was observed again. This was the time when the VR_B entered the lower layer. The lower layer fluid is rolled up in the upper layer (see Fig. 13 (c)). Subsequently, θ decreased while repeating fluctuations and reached a minimum at t^* = 40.3. This is because mixing near the density interface almost stopped (see Fig. 13 (d)). When $t^* > 40.3$, θ gradually decreased with decreasing amplitude. Furthermore, θ also increased and decreased when Δt^* = 16.5 and 22. After θ reached its maximum at $t^* \simeq 12.9$, it reached a minimum at t^* = 27.4 when Δt^* = 16.6 and at t^* = 29.6 when Δt^* = 22. This is because the mixing is not active near the density interface, as shown in Figs. 14 (b) and 15 (b) . Furthermore, it is important to note that these local minima are approximately the same as when Δt^* = 9.6. Specifically, θ exhibited a maximum at t^* = 32.7 when Δt^* = 16.5 and at t^* = 36.5 when Δt^* = 22. This is because the lower layer fluid is rolled up in the upper layer, as shown in Figs. 14 (c) and 15 (c). These maxima are approximately 1.4 times higher than the values at Δt^* = 9.6. The activation of mixing by VR_B was confirmed. Subsequently, θ reached a minimum value. The appearance times were 38.8 and 43.3 for Δt^* = 16.5 and 22, respectively. This is because the lower layer fluid remains slightly above the density interface, as shown in Figs. 14 (d) and 15 (d). However, these local minima were higher than that at Δt^* = 9.6. Hence, the effect of the VR_B was evident. Subsequently, θ gradually decreased. At t^* = 70, θ almost does not depend on Δt^*. In Fig. 16, the experimental results for the single vortex ring as reported by Cao et al., (2019) are also shown by dashed lines. The manner in which θ decreases via repeated increases and decreases is similar to the result of the two vortex rings. The maximum value generated at $t^* \simeq 12.9$ and the value at t^* = 70 were approximately equal. However, at $30 \leq t^* \leq 55$, it was lower than that in the case of two vortex rings. However, it was possible to reconfirm the activation of mixing by the two vortex rings at the same time.

Figure 17 shows the effect of Δt^* on the mixing ability $\hat{\theta}$ calculated from Eq. (2). Here, $t_s = 60d/u_0$. A higher mixing ability is obtained when two vortex rings are injected when compared to that when using a single vortex ring, as shown by the broken line (Cao et al., 2019). However, when Δt^* = 9.6, the difference from a single vortex ring was low. This is because the fluid mass of the 1st vortex ring VR_A that entered the lower layer jets into the upper layer and collided head-on with the subsequent vortex ring VR_B in the vicinity of the density interface. Hence, the penetration depth of the VR_B in the lower layer is low. Conversely, the values of $\hat{\theta}$ at Δt^* = 16.5 and 22 were almost equal, which was approximately 1.4 times higher than that of a single vortex ring. Furthermore, the VR_C, which was generated by the increase in the VR_A from the lower layer, advected upwards from the density interface and collided head-on with the VR_B after its strength decreased. Subsequently, the VR_B continued vertically downward advection and penetrated the lower layer. Furthermore, it levitates and winds the lower layer fluid into the upper layer. Hence, it was determined that under the conditions of this experiment, two vortex rings can effectively mix the upper and lower layers when the time interval $\Delta t^* \geq 16.5$.

4. Conclusions

This study highlighted a two-layer density-stratified fluid filled in a rectangular tank composed of water (upper layer) and aqueous sodium chloride (NaCl) solution (lower layer). Two water vortex rings were intermittently launched vertically downward from the circular orifice (diameter: 10 mm) in the upper fluid toward the density interface. Subsequently, the motion of the vortex rings and behavior of the lower fluid were visualized while the mixing of the upper and lower fluid due to the vortex ring was investigated. The Atwood number (representing the density change at the interface) was 0.0055. Furthermore, the Reynolds number Re, which is based on the circulation of the vortex ring and kinematic viscosity of water, was 1342. Based on the experimental results, the following conclusions were obtained:

1. The 1st vortex ring VR_A advected vertically downward in the upper layer, passed through the density interface, and then advected in the lower layer. The buoyancy acted on the VR_A in the lower layer, which stretched it vertically and reduced the vortex ring diameter. After the VR_A reached the maximum depth in the lower layer, the upper part of the fluid mass ejected into the upper layer due to buoyancy. The lower fluid was entrained in the upper layer. A vortex ring VR_C was generated by the fluid mass ejected in the upper layer and advected vertically upward in the upper layer.
2. The 2nd VR_B collided with the tip of the fluid mass of the VR_A and ejected from the lower layer when Δt^* = 9.6. Subsequently, it slightly penetrated the lower layer, rolled up the lower layer fluid into the upper layer, and coalesced with VR_C to collapse. Furthermore, the VR_B in the case of Δt^* = 16.5 and 22 collided with the VR_C that was rising in the upper layer and then continued to descend to enter the lower layer fluid. Subsequently, the VR_B floated owing to buoyancy and rolled up the lower layer fluid while rising and collapsing. The diameter of the VR_B changes rapidly just before and immediately after the collision with the fluid mass and VR_C.
3. The mixing index of the upper and lower layers reached a maximum at the time when VR_A reached the maximum depth. It also reached a local maximum at the time when the VR_B reached the maximum depth in the lower layer. This was because the upper layer fluid was brought into the lower layer.
4. Under the experimental conditions of this study, the mixing ability at Δt^* = 16.5 and 22 is particularly superior when compared to that for a single vortex ring.

References

Advaith S, Manu KV, Tinaikar A, Chetia UK, Base S (2017) Interaction of vortex ring with a stratified finite thickness interface. Physics of Fluids 29(9):093602, https://dx.doi.org/10.1063/1.4994264

Ansong JK, Kyba PJ, Sutherland BR (2008) Fountains impinging on a density interface. Journal of Fluid Mechanics 595(1):115–139,

https://dx.doi.org/10.1017/s0022112007009093
Bates S, Morrison DS (1997) Modelling the behavior of stratified liquid natural gas in storage tanks: a study of the rollover phenomenon. International Journal of Heat and Mass Transfer 40(8):1875–1884, https://dx.doi.org/10.1016/s0017-9310(96)00218-9
Baines WD, Turner JS, Campbell IH (1990) Turbulent fountains in an open chamber. Journal of Fluid Mechanics 212(1):557–592, https://dx.doi.org/10.1017/s0022112090002099
Bloomeld LJ, Kerr RC (1998) Turbulent fountains in a stratified fluid. J Fluid Mech 358(1):335–356, https://doi.org/10.1017/S0022112097008252
Camassa R, Khatri S, McLaughlin R, Mertens K, Nenon D, Smith C, Viotti C (2013) Numerical simulations and experimental measurements of dense-core vortex rings in a sharply stratified environment. Computational Science & Discovery 6(1):014001, https://dx.doi.org/10.1088/1749-4699/6/1/014001
Cao L, Ito R, Degawa T, Matsuda Y, Takamure K, Uchiyama T (2019) Experimental study of mixing of two-layer density-stratified fluid by a vortex ring. In: Proc. ASME-JSME-KSME 2019 Joint Fluids Engineering Conference, https://doi.org/10.1115/AJKFluids2019-4972
Dahm WJA, Scheil CM, Tryggvason G (1989) Dynamics of vortex interaction with a density interface. Journal of Fluid Mechanics 205(1):1–43, https://doi.org/10.1017/S002211208900193X
Degawa T, Fukue S, Uchiyama T, Ishikawa A, Motoyama K (2017) Behavior of a jet issuing diagonally upward into two-layer density-stratified fluid in a cylindrical tank. Journal of Flow Control, Measurement & Visualization 05(03):51–64, https://dx.doi.org/10.4236/jfcmv.2017.53004
Degawa T, Uchiyama T, Aozasa I, Ishikawa A, Motoyama K (2018a) Numerical simulation of jet issuing diagonally upward into density-stratified fluid in cylindrical tank. Journal of Power and Energy Engineering 06(03):38–52, https://doi.org/10.4236/jpee.2018.63004
Degawa T, Uno K, Uchiyama T (2018b) Mixing of Density-Stratified Fluid in a Cylindrical Tank by a Diagonal Jet. Journal of Energy and Power Engineering 12(9):436–443, https://dx.doi.org/10.17265/1934-8975/2018.09.002
Glezer A (1988) The formation of vortex rings. Physics of Fluids 31(12):3532, https://dx.doi.org/10.1063/1.866920
IEA (2019), Gas 2019: Analysis and Forecasts to 2024, IEA, Paris
Lin YJP, Linden PF (2005) The entrainment due to a turbulent fountain at a density interface. Journal of Fluid Mechanics 542(1):25–52, https://dx.doi.org/10.1017/s002211200500635x
Linden PF (1973) The interaction of a vortex ring with a sharp density interface: a model for turbulent entrainment. Journal of Fluid Mechanics 60(3):467-480, https://doi.org/10.1017/S0022112073000303
Marcus DL, Bell JB (1994) Numerical simulation of a viscous vortex ring interaction with a density interface. Physics of Fluids 6(4):1505–1514, https://dx.doi.org/10.1063/1.868264
Meinke M, Hofhaus J, Abdelfattah A (1998) Simulation of Vortex Ring Interaction. In: E K, K G (eds) IUTAM Symposium on Dynamics of Slender Vortices. Fluid Mechanics and Its Applications, Springer, vol 44
Olsthoorn J, Dalziel SB (2017) Three-dimensional visualization of the interaction of a vortex ring with a stratified interface. Journal of Fluid Mechanics 820:549–579, https://dx.doi.org/10.1017/jfm.2017.215
Robins RE, Delisi DP (1998) Numerical Simulation of Three-Dimensional Trailing Vortex Evolution in Stratified Fluid. AIAA J 36:981–985, https://doi.org/10.2514/2.468
Stock MJ, Dahm WJ, Tryggvason G (2008) Impact of a vortex ring on a density interface using a regularized inviscid vortex sheet method. Journal of Computational Physics 227(21):9021–9043, https://dx.doi.org/10.1016/j.jcp.2008.05.022
Tsunoda H, Hosaka M, Amano S (2011) Visualization of a Round Vortex Ring Interacting with a Density Interface. Transaction of the Visualization Society of Japan 31(7):21–26, https://dx.doi.org/10.3154/tvsj.31.21

Uchiyama T, Kusamichi S (2017a) Control of Air Bubble Cluster by a Vortex Ring Launched into Still Water. International Journal of Chemical Engineering and Applications 8(1):37–46, https://dx.doi.org/10.18178/ijcea.2017.8.1.628

Uchiyama T, Yano C, Degawa T (2017b) Generation and Transport of Solid Particle Clusters Using a Vortex Ring Launched into Water. International Journal of Chemical Engineering and Applications 8(4):253–260, https://dx.doi.org/10.18178/ijcea.2017.8.4.666

Table 1 Experimental conditions

Density-stratified fluid	Water/NaCl aqueous solution
Orifice diameter d	10 mm
Atwood number A	0.0055
Reynolds number Re	1342
Froude number Fr	0.11
Richardson number Ri	0.049
Time interval for injection of vortex ring Δt^*	9.6, 16.5, 22

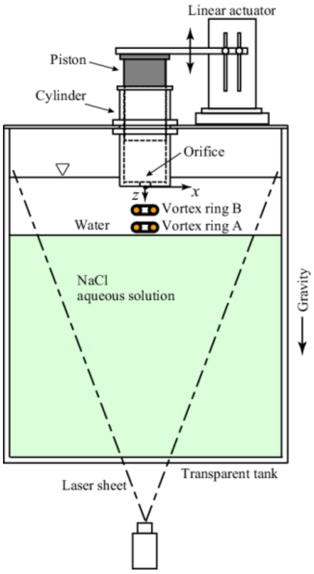

Fig. 1 Schematic of the experimental set-up

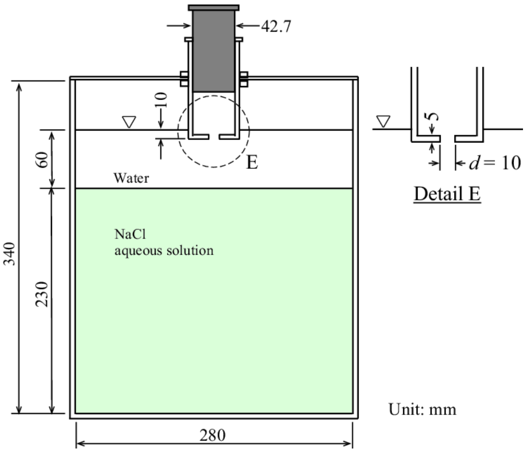

Fig. 2 Structural dimensions of the experimental apparatus

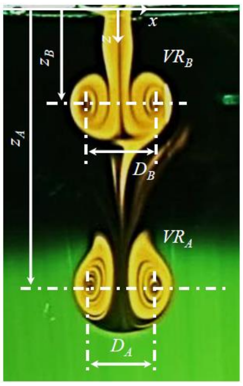

Fig. 3 Displacement and diameter of the vortex rings

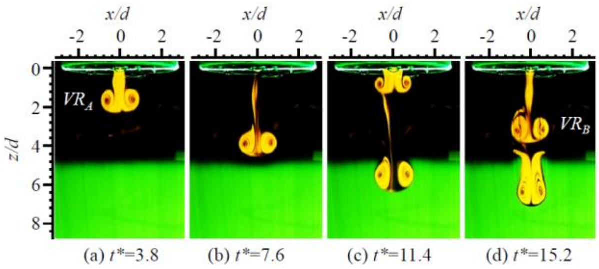

Fig. 4 Images of vortex rings and lower fluid at $3.8 \leq t^* \leq 15.2$ in the case of $\Delta t^* = 9.6$

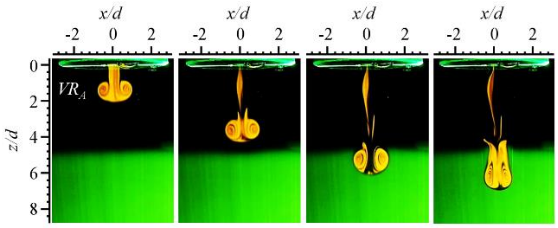

(a) t^*=3.8 (b) t^*=7.6 (c) t^*=11.4 (d) t^*=15.2

Fig. 5 Images of vortex ring and lower fluid at $3.8 \leq t^* \leq 15.2$ in the case of $\Delta t^* = 16.5$

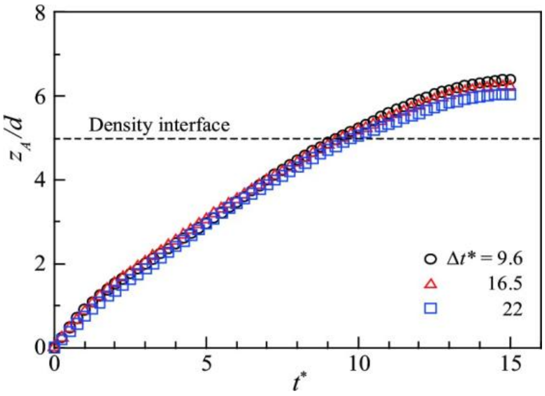

Fig. 6 Time-variation of the displacement of the 1st vortex ring VR_A

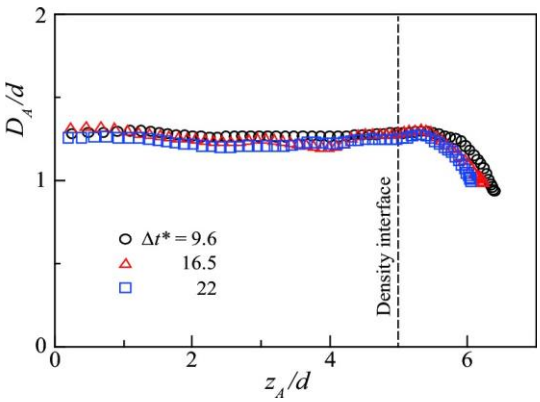

Fig. 7 Time-variation of the diameter of the 1st vortex ring VR_A

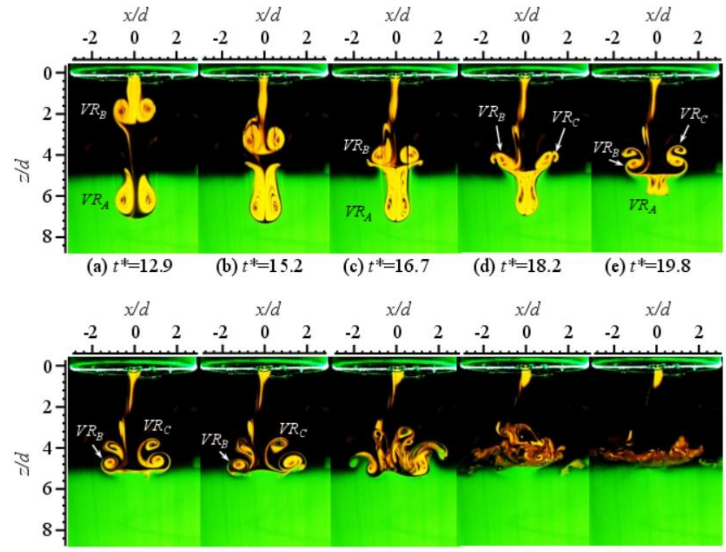

(a) t^*=12.9 (b) t^*=15.2 (c) t^*=16.7 (d) t^*=18.2 (e) t^*=19.8

(f) t^*=21.3 (g) t^*=22.8 (h) t^*=26.6 (i) t^*=40.3 (j) t^*=63.1

Fig. 8 Images of VR_A, VR_B and lower fluid in the case of $\Delta t^* = 9.6$

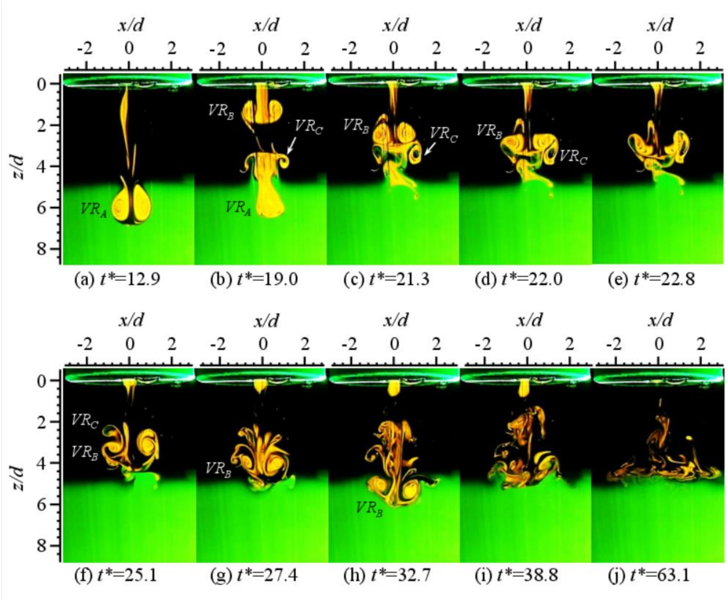

Fig. 9 Images of VR_A, VR_B and lower fluid in the case of $\Delta t^* = 16.5$

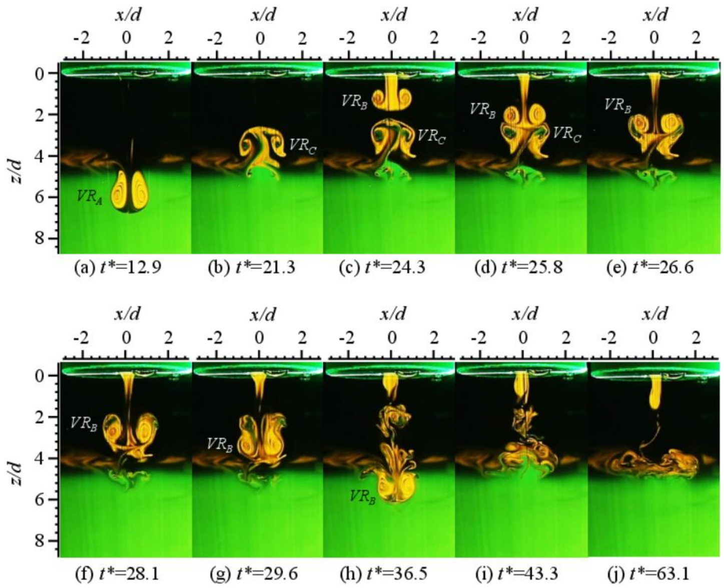

Fig. 10 Images of VR_A, VR_B and lower fluid in the case of $\Delta t^* = 22$

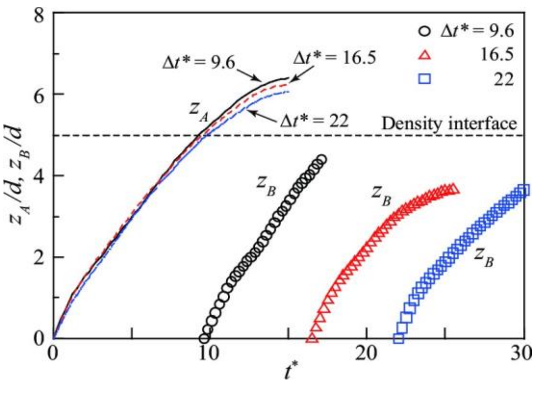

Fig. 11 Time-variation of the displacement of the 2nd vortex ring VR_B

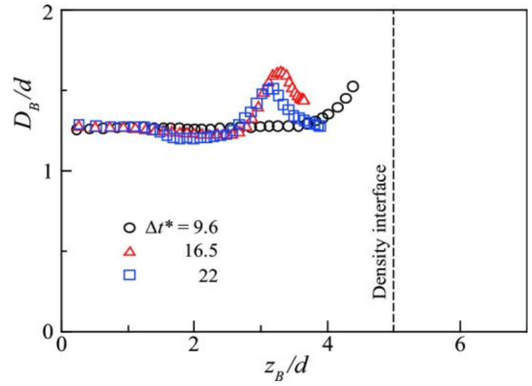

Fig. 12 Time-variation of the diameter of the 2nd vortex ring VR_B

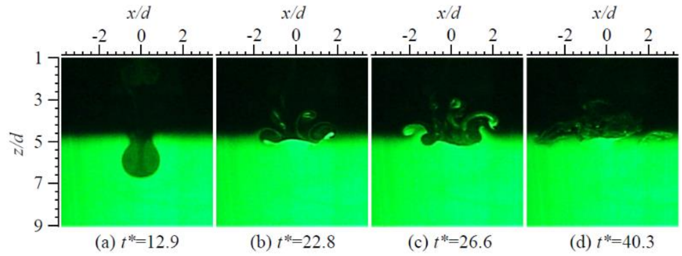

Fig. 13 Images of lower fluid in the case of $\Delta t^* = 9.6$

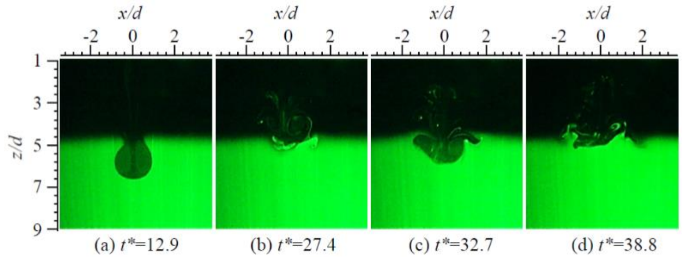

Fig. 14 Images of lower fluid in the case of $\Delta t^* = 16.5$

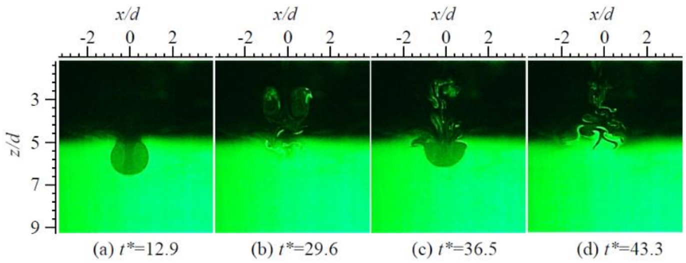

Fig. 15 Images of lower fluid in the case of $\Delta t^* = 22$

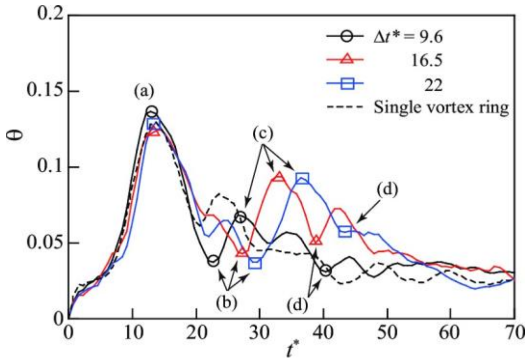

Fig. 16 Time-evolution of the mixing index θ

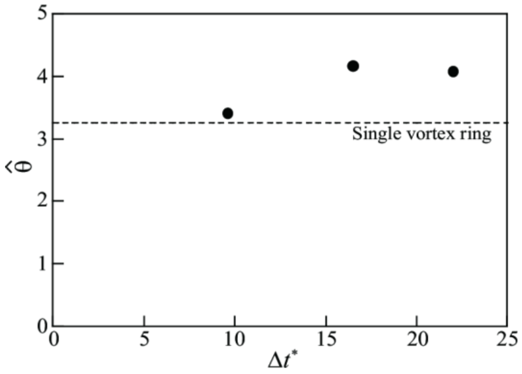

Fig. 17 Effect of Δt^* on the mixing ability $\hat{\theta}$